JOURNAL OF APPLIED PHYSICS 119, 023104 (2016)

Experimental demonstration and modeling of the internal light scattering profile within solar cells due to random dielectric scatterers

Joseph Murray and Jeremy N. Munday[a)]
Department of Electrical and Computer Engineering, University of Maryland, College Park, Maryland 20742, USA and Institute for Research in Electronics and Applied Physics, University of Maryland, College Park, Maryland 20740, USA

(Received 11 November 2015; accepted 24 December 2015; published online 13 January 2016)

Many photovoltaic technologies are shifting toward thin-film devices to simultaneously reduce costs and improve carrier collection efficiencies; however, the need for nearly complete light absorption within the semiconductor to achieve large short-circuit currents constrains this thickness reduction. Light trapping strategies can be employed to increase absorption in thinner devices. Random scattering coatings offer a simple, cost-effective way to increase solar cell absorption without the drawback of increased surface recombination or reduced bandwidth that occurs when using surface texturing or gratings. However, coatings that show excellent performance as scatterers in free space generally do not enhance device absorption as much as an ideal Lambertian scatterer. Here, we present an experimental technique and theoretical model that accurately describes the absorption improvement that is achievable with coatings based on random ensembles of dielectric scatterers. We find that the ideal Lambertian model substantially overestimates the experimental scattering results, but significant path length enhancements are still achievable. The experimental techniques presented here should enable the testing of various optical models that attempt to surpass the ray optics light trapping limit, which have in many cases been hindered by the experimental difficulty of coupling the incident light into the optical modes of the absorber. © *2016 AIP Publishing LLC*. [http://dx.doi.org/10.1063/1.4939646]

I. INTRODUCTION

Minimization of the device thickness is an important goal in photovoltaic designs as it generally lowers costs and reduces bulk recombination losses. The drawback of thinner devices is lowered absorption; however, by employing light trapping, this fundamental trade-off can be circumvented. An enormous variety of strategies have been experimentally and theoretically investigated. These approaches include texturing,[1] plasmonic nanoparticles,[2,3] gratings,[4–6] nanowires,[7,8] nanocones,[9–11] dielectric particle arrays,[5] etc. Many of these techniques require lithography, high temperature processing, or hazardous chemicals and are hampered by high surface recombination.[12] A cost effective and simple alternative is the addition of random dielectric nano- or micro-scatterers. These may be easily applied as a back-side reflector/scatterer and have been shown to be effective for light trapping.[13–16]

To properly design and optimize cells using these random dielectric nanoparticle reflectors, a detailed understanding of their scattering properties is required. There is a large body of literature on scattering in diffuse materials.[17,18] Much of it is concerned with calculating the fractions of scattered and directly transmitted light in the diffuse medium rather than its angular distribution and it is usually assumed that the mean free path is much greater than the wavelength of light, which is not the case for densely packed wavelength-sized particles. Calculations have also been done outside of this low density regime using Monte Carlo simulations,[19] N-flux radiative transfer method,[20] a 1-D semi-coherent method,[16] and more recently rigorous coupled wave analysis[21] in order to determine the fractions of scattered and direct light in diffuse media. However, often the scattering material is dense, randomization is assured, and the internal scattering of the diffuse media is not the primary concern. In such cases two models are generally used to describe or compare the absorption due to these scatterers: either the material is taken to produce Lambertian scattering from the back side of the absorber or it is assumed that within the scattering material the light is fully randomized but is limited by a critical angle as it enters the absorber.[22] Neither of these models accurately describes the actual scattering in the cell. One way to improve the modeling would be to measure the scattering distribution inside the absorber, but this measurement is not in general possible with planar structures due to a portion of the light experiencing total internal reflection.

Here we present an improved characterization method that uses a hemispheric lens and reflectometry to extract information about the internal scattering distribution. With the scattering distribution known, we are able to reassess the scattering models. We use this method and improved modeling to demonstrate the importance of the interface between the scatterer and absorber in determining the resulting absorption. We find that the scattering distribution is best described by an ensemble of effective indices at the absorber/scatterer boundary. Finally, we demonstrate the accuracy of this technique by comparing its predictions to

a)Electronic mail: jnmunday@umd.edu

 © 2016 AIP Publishing LLC

[This article is copyrighted as indicated in the article. Reuse of AIP content is subject to the terms at: http://scitation.aip.org/termsconditions. Downloaded to] IP: 73.212.41.40 On: Sat, 16 Jan 2016 13:42:15

several experimental configurations. We find that our procedure allows for high accuracy predictions of absorption based on our measured scattering data.

II. MODELING OF RANDOM DIELECTRIC SCATTERERS

One of the simplest approaches to model scattering inside a slab or film is to assume perfect reflection off the back surface and complete randomization of the incident light (Fig. 1(a)). This model results is the well-known Lambertian scattering intensity distribution of $I_o \cos(\theta)$ in units of power per unit area per steradian, where θ is the angle from the surface normal. This expression is derived from simple geometric considerations assuming photons are equally likely to be reflected in any direction. If the sample has a back reflector and can support a large number of modes (approaching a continuum), the Lambertian distribution results in absorption given by[23]

$$A \cong \frac{(1 - e^{-4\alpha h})T_{in}}{\left(1 - e^{-4\alpha h}\left(1 - \frac{\bar{T}_{esc}}{n_{abs}^2}\right)\right)}, \tag{1}$$

where α is the absorption coefficient, h is the thickness of the absorbing layer, n_{abs} is the index of refraction of the absorbing layer, and T_{in} is the incident transmitted fraction at the top interface. $\bar{T}_{esc}$ is the weighted transmitted fraction of light exiting from the slab through the escape cone (defined as $\bar{T}_{esc} = 2n_{abs}^2 \int_0^{\sin^{-1}(1/n_{abs})} T_{esc}(\theta)\cos(\theta)\sin(\theta)d\theta$, where T_{esc} is the transmission coefficient). For an ideal antireflection coating, we can also make the approximation $T_{in} = \bar{T}_{esc} \approx 1$ to further simplify Eq. (1). For a thick material (i.e., $h \gg \lambda$) with weak absorption ($\alpha h \ll 1$), e.g., in bulk silicon near the bandgap, the absorbed fraction reduces to the well-known $4n^2$ limit[24,25]

$$A \approx 4{n_{abs}}^2\alpha h. \tag{2}$$

The Lambertian model however is only a simple model for scattering and poorly describes real dielectric scatterers. New models are needed in order to determine the scattering properties, and hence the absorption, that result from real dielectric back scatterers. An improved model assumes that light inside the scattering material is fully randomized but can only emit into the absorber through a fraction of the full 2π steradians. This fraction is determined by the critical angle defined by the index contrast between the sample, n_{abs}, and the binder or filler of the dielectric scatterer, n_b.[13,22] This scattering distribution is sometimes referred to as a focused Lambertian distribution and is given, again in units of power per unit area per steradian, by

$$\begin{aligned} I(\theta) &= \mathrm{I}_o \cos(\theta)\left(\frac{n_{abs}}{n_b}\right)^2 \quad \text{for} \quad \theta < \sin^{-1}\left(\frac{n_b}{n_{asb}}\right) \\ \mathrm{I}(\theta) &= 0 \qquad\qquad\qquad\quad \text{for} \quad \theta > \sin^{-1}\left(\frac{n_b}{n_{asb}}\right). \end{aligned} \tag{3}$$

This equation is derived from the assumptions above by mapping angles from inside the scatterer to inside the absorber using Snell's law. Note that this formula is only valid when $n_b < n_{abs}$. If this condition is not satisfied, further scattering into evanescent and surface modes may occur and further increase the absorption. For $n_b < n_{abs}$, this distribution results in absorption less than the *$4n^2$ limit*. Under the same assumptions used to derive the *$4n^2$ limit*, the absorption can be approximated as

$$A \approx 2Khn_b^2, \tag{4}$$

where K is the effective absorption coefficient defined by

$$K \equiv \frac{-\ln(1 - \bar{A})}{h}, \tag{5a}$$

where

$$\bar{A} \equiv 2\frac{n_{abs}^2}{n_b^2}\int_0^{\theta_c}\left[1 - \exp\left(\frac{-\alpha h}{\cos(\theta)}\right)\right]\cos(\theta)\sin(\theta)d\theta \tag{5b}$$

and

$$\theta_c = \sin^{-1}\left(\frac{n_b}{n_{abs}}\right). \tag{5c}$$

Here, $\bar{A}$ is a weighted average of the absorption due to different ray optic paths.[22] When the absorption cannot be calculated under these simplifying equations, a more complex system of equations must be solved. This calculation is typically performed using the so-called four flux method.[20,22] In Section IV, we present a modified version of this method.

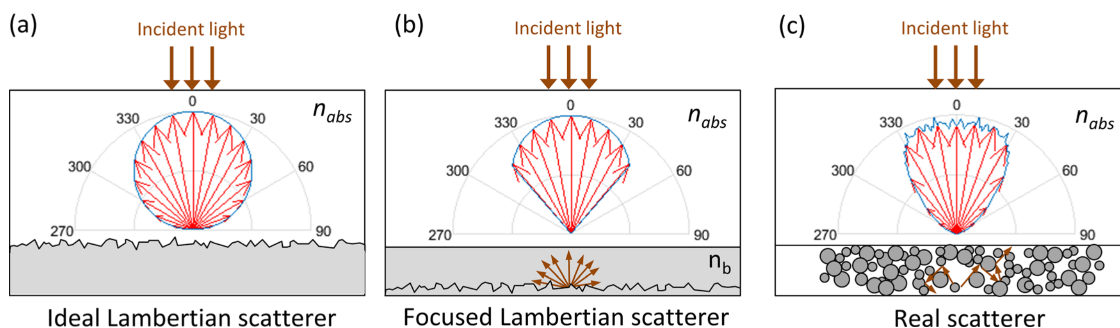

FIG. 1. Scattering profiles within an absorbing slab of refractive index n_{abs} for (a) an ideal Lambertian scatterer, (b) a focused Lambertian scatterer, and (c) a real scatterer consisting of barium sulfate particles on the back of a GaP substrate.

[This article is copyrighted as indicated in the article. Reuse of AIP content is subject to the terms at: http://scitation.aip.org/termsconditions. Downloaded to] IP: 73.212.41.40 On: Sat, 16 Jan 2016 13:42:15

While the focused Lambertian model described above offers improvements over the Lambertian scattering model, neither is able to reproduce the scattering profile of real dielectric scatterers (Fig. 1). The Lambertian distribution is often used because it leads to simple closed form solutions[23,24] and serves as a common benchmark. Further, the scattering distribution of high quality dielectric scatterers can be very nearly Lambertian when light is incident on the coating from air.[16,26] However, for real dielectric scatterers attached to the back of an absorbing slab, the scattering profile deviates from the Lambertian distribution because the scattering actually occurs partially outside of the absorbing slab. This situation also implies that there is a critical angle beyond which scattering cannot occur, which leads to the focused Lambertian model (Fig. 1(b)). This model assumes that the light is impinging on the absorbing slab from a material of refractive index n_b. In reality, a fraction of the light will be impinging on the absorbing material directly from the scattering particles (see, for example, the inset in Fig. 2(a)), which have an index of refraction that is different from n_b. Although only a small fraction of the absorber's surface is touching the scattering particles, it can have a large impact on the total absorption because light incident on the absorber from the high index scatterer will have longer path lengths on average, which are more likely to lead to absorption.[27] Figure 2 compares the absorption resulting from both a Lambertian scattering model and a focused Lambertian scattering model to experimental results (absorption is directly measured with an integrating sphere; details in Section IV) from a GaP slab with barium sulfate scattering particles attached to the backside to illustrate the importance of accounting for the scattering into these larger angles. Here, the Lambertian distribution greatly overestimates the actual absorption, while the focused Lambertian greatly underestimates the actual absorption. It should be noted that the focused Lambertian may be modified by using n_b as a fitting parameter to describe an effective index; however, our goal is to accurately predict the measured absorption a priori. Furthermore, if n_b is used as a fitting parameter, different values of n_b may be obtained for different absorber/substrate configurations, offering minimal physical insight into the scattering and absorption phenomena.

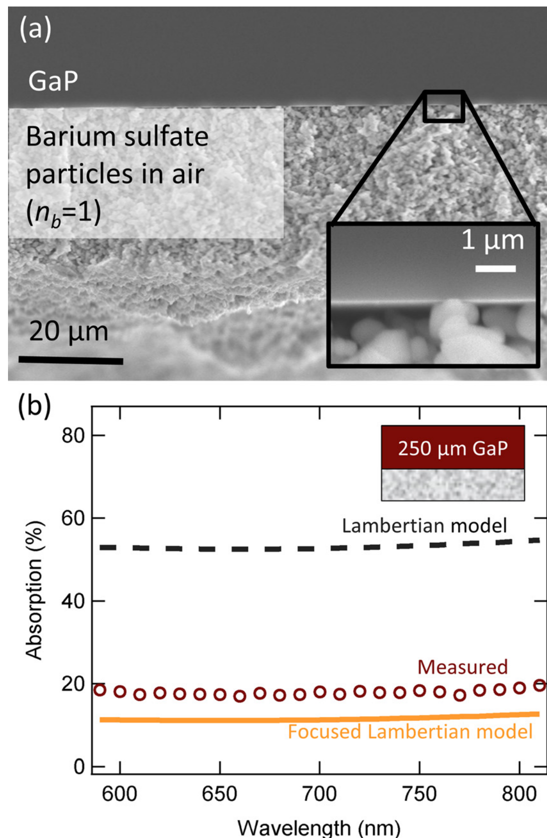

FIG. 2. (a) SEM cross-section of the GaP absorbing slab and a thin layer of barium sulfate scattering particles (actual samples have scattering layers with thickness on the order of a millimeter). Inset shows that a majority of the GaP surface is in contact with air, while a small fraction of the surface is in contact with the high index barium sulfate particles. (b) Calculated and measured absorption in a 250 μm slab of GaP with weak, but not insignificant, absorption beyond the bandgap (550 nm) for the sample shown in (a). The calculations are shown for either a Lambertian or a focused Lambertian (with $n_b = 1$) scattering distribution at the rear of the slab. Both models are in poor agreement with experimental data.

III. MEASUREMENT OF THE SCATTERING PROFILE WITHIN A MATERIAL

There are several common approaches to measuring angularly resolved reflection from a scattering surface. The simplest method is to deposit the scattering material on a substrate and illuminate the air/scatterer interface. The scattering distribution is then obtained by measuring the scattered light as a function of angle. This measurement can accurately describe light reflected at the interface of the scattering surface and the air; however, it does not provide information about how light would scatter into an absorbing slab placed on top of the scattering surface. The scattering of light into an absorbing slab is different than the scattering into free-space. If the same technique was applied to an absorbing slab with a back scatterer, the measured scattering distribution would only detect the radiation modes (i.e., light that exits the slab through the critical angle, $\theta_c = \arcsin(1/n_{abs})$) and would neglect the trapped modes (i.e., modes that correspond to ray-optic paths that lay outside of the critical angle), as demonstrated in Fig. 3(a). Because only light within the critical angle of the slab can escape, no information is obtained by the photo-detector about light that was scattered into larger angles. A simple solution is to replace the slab with a hemisphere that allows for all scattered angles to exit the material and be collected by the detector (Fig. 3(b)). The two main limitations of this experimental method are that (i) a hemisphere with low absorption is required for the index of refraction and wavelength of interest, and (ii) the scattering layer should not generate significant surface waves, because they will not propagate to the far field and will thus not be detected.

To completely characterize the scattering distribution, detection of all scattered light is required. This can be accomplished with the use of a hemispheric lens (Fig. 3(b)). The minimum hemisphere radius required to ensure sampling of all scattering angles is

$$R > rn, \tag{6}$$

[This article is copyrighted as indicated in the article. Reuse of AIP content is subject to the terms at: http://scitation.aip.org/termsconditions. Downloaded to] IP: 73.212.41.40 On: Sat, 16 Jan 2016 13:42:15

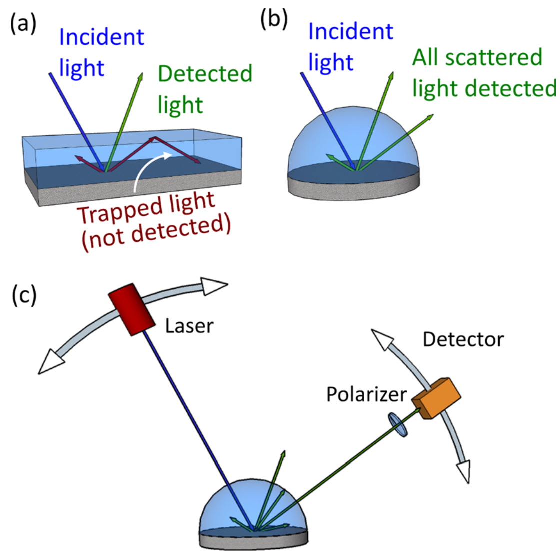

FIG. 3. Schematic showing the collection of scattered light (a ray optics configuration is shown for simplicity). (a) A slab with a scattering medium adhered to the back. Some scattered rays are not detected as a result of light trapping. Similarly, the maximum angle of incidence on the rear reflector is limited to the critical angle. (b) A hemisphere with a scattering medium on the back surface. All incidence angles are accessible and all scattered angles can be detected. (c) Schematic of the gonioreflectometer measurement setup used in our experiments.

where R is the radius of the half sphere and r is the radius of the illuminated spot size.[28] However, in practice R should be significantly larger than the product rn to avoid lensing effects. In the ideal case, multiple scattering events would be eliminated with an appropriate anti-reflection coating.

Scattering measurements are made using a custom gonioreflectometer with sample illumination by a HeNe laser (Fig. 3(c)). For a given laser beam polarization, the detector is rotated about the sample and the signal is measured by a silicon photodiode using a Keithley 2400 Sourcemeter. A polarizer is placed in front of the detector and is either aligned or anti-aligned with the laser to separate diffuse and specular reflection/scattering. The polarizing filter has an extinction ratio of ∼10 000. When the specular intensity per unit solid angle is less than 10 000 times the diffuse intensity per unit solid angle, the specular portion is effectively removed by the polarizer. This condition holds true for most of the data of interest but is easily violated when very little scattering occurs such as when the angle of the incident light exceeds the critical angle between the glass/scatterer (see further discussion below). Measurements are made for both polarizations and are similar in all scattering measurements. Samples are prepared by depositing scattering materials onto BK7 ($n = 1.51$) or S-LAH79 ($n = 2.0$) glass hemispheres. The scattering coatings were prepared using a commercially available barium sulfate micro-particle solution (Avian B) per the manufacturer's instructions. These coatings were made ∼1 mm thick to eliminate transmission. Particle size, determined by SEM (see Fig. 2(a)), was found to range from 100 s of nanometers to a few microns.

Measurements of optical scattering by white paint (randomly packed barium sulfate particles) at the air/paint interface show equal scattering in all directions and is well described as a Lambertian scattering material (Fig. 4(a)). When this same diffuse reflector is applied to the back interface of a BK7 glass hemisphere, the measured angular distribution is significantly different. Specifically, less light is scattered at large angles, which results in insufficient light trapping and hence reduced absorption compared to what would have been predicted based on a Lambertian scattering profile.

In order to better understand the scattering produced by the white paint when the interface is not air, we measure and analyze the scattering distribution for two different glass hemispheres (BK7 and LAH79) as a function of incident illumination angle (Fig. 5(a)). Light is scattered efficiently up to an effective critical angle (∼42° in BK7 and ∼30° in S-LAH79), beyond which a reduced amount of scattering extends to nearly 90° (Fig. 5(b)). Scattering into a high index hemisphere (S-LAH79 with $n = 2.0$) has many of the same general features demonstrated with the low index hemisphere (BK7 with $n = 1.51$), but there is a much smaller critical angle (∼30°) due to the increased refractive index contrast between the hemisphere and the scattering material.

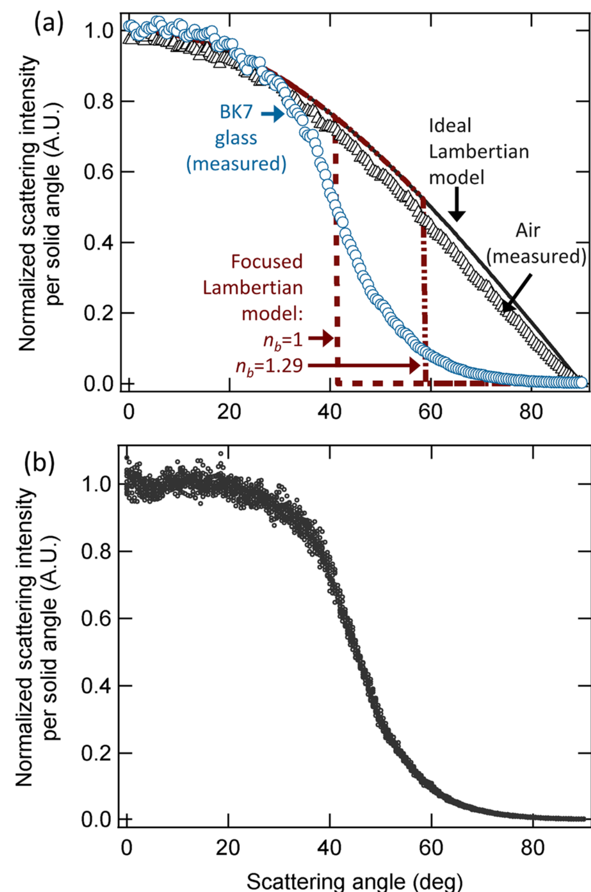

FIG. 4. (a) Measured scattering intensity for illumination at 10° incidence at the interface of barium sulfate scatterers and air (triangles) or BK7 glass (circles) compared to the ideal Lambertian scattering model (solid line) and the focused Lambertian model (dashed lines), for laser illumination at $\lambda = 633$ nm (HeNe laser). Shown also are the calculated focused Lambertian distributions with an effective index of either 1 (air) or 1.29 (the effective index which produces the closest fit to the absorption data in Figure 2(b)). (b) Overlapping measured scattering distributions for incident illumination from 5° to 35°. The close overlap between these traces demonstrates full randomization in the scattering material.

[This article is copyrighted as indicated in the article. Reuse of AIP content is subject to the terms at: http://scitation.aip.org/termsconditions. Downloaded to] IP: 73.212.41.40 On: Sat, 16 Jan 2016 13:42:15

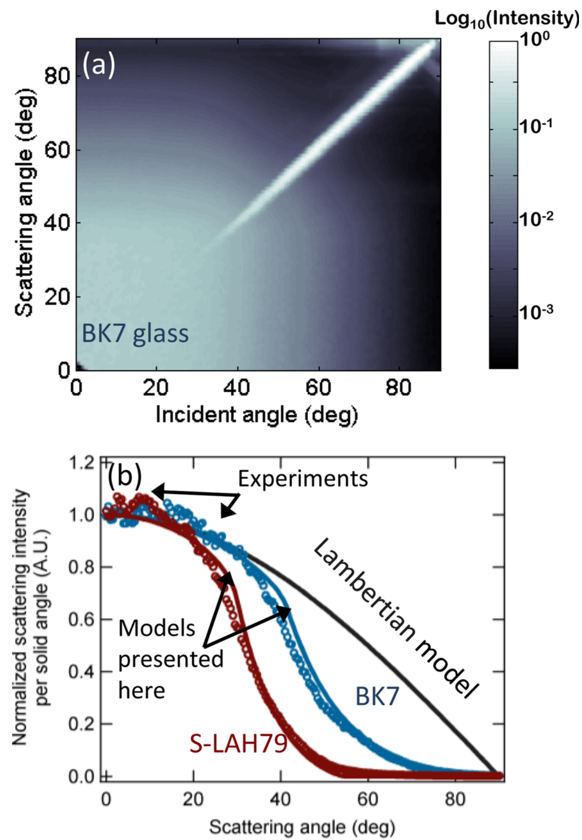

FIG. 5. (a) Normalized scattering intensity measurements (log scale) using a BK7 glass hemisphere. (b) The scattering intensity for an input angle of 10° shows that our model agrees well with the experimental data for both BK7 and S-LAH79 samples. Here, the model was fit for the BK7 sample and confirmed by the measurement using the S-LAH79 sample.

In addition, while the scattering in the BK7 hemispheres extends to nearly 90°, the scattering into the S-LAH79 glass approaches zero much more quickly. (Note that the scattering distribution appears to narrow in Figure 5(a) beyond the critical angle mentioned above (∼42°). This apparent narrowing is simply due to the finite extinction ratio of the polarizer (the specular reflection becomes very large) and is not due to an increase in the diffuse scattering).

A focused Lambertian model would predict the observance of a critical angle defined by the effective index of the scatterer and the glass hemisphere, but not the extended tail shown in Fig. 4(a) for any effective index. In fact if an effective index is used to fit the data from Fig. 2(b) (found to be 1.29 for a best fit to the absorption data) the resultant focused Lambertian distribution (shown in Fig. 4(a)) poorly matches the scattering data. A possible explanation for the observed scattering distribution is that the light entering the scatterer is not fully randomized. However, Fig. 4(b) plots overlapping normalized scattering distributions for incident illumination angles from 5° to 35°. If light were not randomized within the scattering layer, the resulting scattering profile would depend on the incident angle. Instead the scattering is nearly independent of incident angle, having a relative standard deviation of less 4% over this angular range. We thus posit that the measured data are best described by an ensemble or mixture of effective indices at the dielectric/scatterer interface. This interpretation is also suggested by the SEM images in Fig. 2. While much of the interface on the microscopic scale is occupied by interstitial air, some areas are contacted by the barium sulfate particles directly. This heterogeneity leads to variety of effective indices of the scattering material and each index allows for scattering into a subset of angles in the dielectric half sphere.

To test this hypothesis, we first calculate what this index ensemble would be in order to correctly describe the scattering into the BK7. Here we allow the effective index to be randomly chosen from a generating function bounded by 1 (index of air) and 1.63 (index barium sulfate). The resultant scattering distribution given in units of intensity per unit solid angle is

$$I(\theta) = I_0 \cos(\theta) \left\langle T(\theta) P(n_{eff}) \left(\frac{n_{abs}}{n_{eff}}\right)^2 \right\rangle_{n_{eff}}, \quad (7)$$

where θ refers to the angle from normal inside the dielectric, n_{eff} is the effective index ensemble of the scattering material, $T(\theta)$ is the transmission coefficient into the dielectric, $P(n_{eff})$ is the probability of scattering from a given effective index, and $\langle\rangle_{n_{eff}}$ indicates the average over the ensemble. The fit is determined by minimizing the root mean squared (RMS) error between the measured scattering data and $I(\theta)$. Note that the scattering intensity defined above is valid under the assumptions that the scattering layer completely randomizes the light, does not contribute significantly to the absorption, and the scatterer has a negligible imaginary part of the refractive index. Thus, the model is independent of the size (microscale or macroscale) of the individual index domains, so long as the light is randomized. The scattering may also be wavelength dependent due to particle size or dispersion in the refractive index of the materials; however, both of these effects are accounted for by a wavelength dependent transmission coefficient and scattering probability. For cases where the index contrast between the particles and the surrounding medium is low or the particles are large, thicker films may be necessary to ensure randomization.

Once the index ensemble is determined from the measured scattering into the BK7 half sphere, as described above, the model is compared to the measured data obtained using a S-LAH79 hemisphere, which as a different index of refraction. Figure 5(b) compares the measured data to this model. The index ensemble model is in good agreement with the measured result correctly predicting the sharp roll-off at the air/glass critical angle (30°), the extended tail, and the lack of scattering beyond the air/barium sulfate critical angle (∼55°). This agreement strongly suggests that the index ensemble interpretation can be used to accurately model the scattering. Further, the agreement of our model with measured data from a hemisphere with a different index of refraction supports the interpretation of the index ensemble model as a physically meaningful description of the scattering layer. To ensure the most accurate index ensemble model, the measured intensity data should be obtained using a hemisphere whose index of refraction is equal to or larger than the maximum index used in the model ($n = 1.63$ in our case). However, this requirement is often not necessary, as the model obtained from the BK7 ($n = 1.51$) hemisphere

[This article is copyrighted as indicated in the article. Reuse of AIP content is subject to the terms at: http://scitation.aip.org/termsconditions. Downloaded to] IP: 73.212.41.40 On: Sat, 16 Jan 2016 13:42:15

scattering profile was able to accurately describe the scattering within the S-LAH79 material ($n = 2.0$). In Sec. IV, this conclusion is tested further with a greater range of structures.

IV. MEASURED AND CALCULATED ABSORPTION

To further validate this model and demonstrate its utility, we make absorption measurements for a variety of samples with random barium sulfate nanoparticle back reflectors. These measurements are made using an integrating sphere (Labsphere RTC-060) with incident illumination at 13° from normal. Samples are placed in the center of the sphere and are directly illuminated. This technique allows for a direct measurement of absorption by simultaneously collecting all reflected and transmitted light (both direct and scattered) and subtracting it from the total incident light. Second order diffuse absorption in the sample (light reflected from the sample then absorbed after scattering from the wall of sphere) is corrected for by measuring diffuse absorption through a secondary port. ITO is used as a low index absorber, GaP as a high index absorber, and glass as a minimally absorbing substrate. Measurements of samples using a GaP substrate are made at wavelengths greater than the bandgap of GaP to avoid complete absorption in the GaP prior to scattering off the back reflector. Measurements for ITO on glass are made at shorter wavelengths to ensure sufficient absorption (ITO absorption typically peaks in the near UV). Film thicknesses are measured by AFM (Asylum Research, Cypher) and confirmed by ellipsometry (J.A. Woollam M-2000D). The refractive index of the films and substrates is measured by ellipsometry. We note that ellipsometry cannot accurately determine the very small imaginary parts of the refractive index for glass and GaP samples. These small values (10^{-6}–10^{-8}) are calculated based on separate absorption measurements of those materials alone (no back-scatterers) using the integrating sphere setup. The dielectric scatterers are applied to the absorbers in the same manner as in the scattering measurements. The absorption loss per reflection of the scattering layer is characterized by absorption measurements with illumination on the air/scattering interface. Note that the transmission through these scattering layers is found to be much less than 1% so that any reflection less than unity can be attributed to absorption in the scattering layer.

Absorption measurements for the full structures (scattering material on film/substrate) are compared to the calculated absorption based on the index ensemble model. Absorption is calculated by a modified version of the four flux method following Cotter.[22] Here, based on the measurements shown in Figure 4(b), we assume that all light entering the scattering material is completely randomized. Thus, in contrast to the typical implementation of the four-flux method, the fraction of light scattered (not specular reflection) at the absorber/scatterer interface is simply determined by Fresnel coefficients (using an index ensemble). All transmission and reflection coefficients are calculated by the matrix transfer method including coherent (thin films) and incoherent (thick substrates) reflections/transmissions following Katsidis and Siapkas.[29] All such coefficients were found for light passing through the entire film/substrate stack. Thus, the multiple reflections inside of the film/substrate are automatically accounted for using this method. The total absorption is calculated as the fraction of light that does not escape from the front surface of the sample and is given by

$$A = 1 - \left[\langle R_{dir,in} \rangle_{n_{eff},s/p} + \frac{\rho_{\mathrm{int}} \langle P(n_{eff}) T_{dir,in} \rangle_{n_{eff},s/p} \langle P(n_{eff}) T_{diff,\mathrm{out}} \rangle_{n_{eff},s/p}}{1 - \rho_{\mathrm{int}} \langle P(n_{eff}) R_{diff,\mathrm{out}} \rangle_{n_{eff},s/p}} \right], \quad (8)$$

where $\langle \rangle_{n_{eff},s/p}$ denotes averaging over the index ensemble (as determined from the scattering data) and both polarizations (note: while we assume the polarization is randomized by the scattering, the transmission and reflection coefficients are still polarization dependent). ρ_{int} is the absorption loss per reflection of the scattering material itself. $R_{dir,in}$ ($T_{dir,in}$) is the reflection (transmission) coefficient of direct illumination passing through the sample to the scatterer. $R_{diff,\mathrm{out}}(T_{diff,\mathrm{out}})$ is the total integrated diffuse reflection (transmission) coefficient for light traveling from the scatterer through the sample to air. These values can be calculated from the angularly dependent reflection (transmission) coefficient, $R_{out}(\theta)$ ($T_{out}(\theta)$), by

$$R_{diff,out} = 2 \int_0^{\pi/2} R_{out}(\theta_{scat}) \cos(\theta_{scat}) \sin(\theta_{scat}) d\theta. \quad (9)$$

Here, θ_{scat} is the angle from the normal in the scattering material (not the angle of the light escaping the surface). Note that determining the effective index ensemble is critical for our calculation in two ways. First, it allows for accurate modeling of the scattering profile. Second, it allows for calculation of the appropriate Fresnel coefficients. As a result, the increase in absorption due to light trapping can be fully modeled, even in thin-films.

Figures 6(a)–6(c) show that the measured absorption is well described by the ensemble model. For all of the measurements, the models have an RMS error of <1.5% (with 0.9%, 1.4%, and 1.4% for the GaP (6a), the dual-layer GaP/ITO (6b), and the dual-layer Glass/ITO (6c) samples, respectively). We attribute the greater error in the ITO samples to the large variability in ITO index, resulting in less accurate fits to the ellipsometry data. In all cases, the Lambertian model greatly overestimates the absorption and the focused Lambertian greatly underestimates the absorption. These results demonstrate the utility and versatility of the index ensemble model and further support our interpretation of the underlying physics.

These measurements also illustrate some important points about scattering and absorption in general. First note that there is significant absorption in the GaP (6a) sample despite the miniscule intrinsic absorptivity of this material (in this wavelength range). This absorption is primarily due to the high refractive index of the GaP. The large index results in high reflection for light attempting to escape the GaP (increased path length) and in high reflection for light entering the GaP from the scatterer (high loss in the scatterer; ~1/3 the total loss in this case). Also note the relatively small difference in

[This article is copyrighted as indicated in the article. Reuse of AIP content is subject to the terms at: http://scitation.aip.org/termsconditions. Downloaded to] IP: 73.212.41.40 On: Sat, 16 Jan 2016 13:42:15

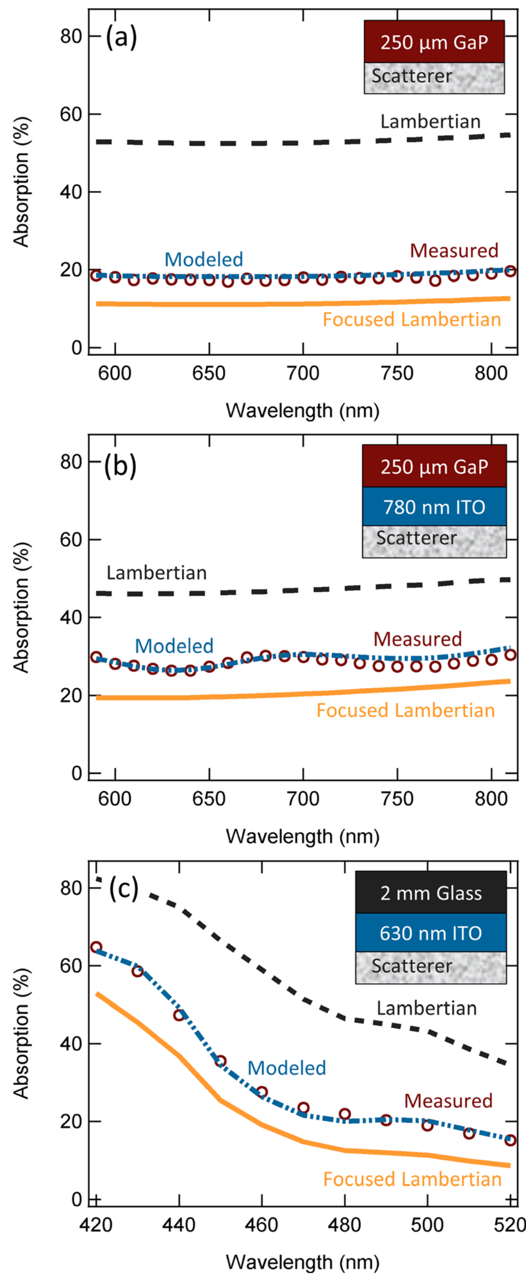

FIG. 6. Absorption measurements accurately modeled. (a) Same data as Figure 2(b) including the scattering modeled using the index ensemble model. The RMS error between measurement and calculation is 0.9%. (b) An interstatial ITO layer is added to manipulate the scattering rate and increase the absorption. Here the RMS error is 1.0%. Note the reduced absorption for the Lambertian model is due to the lower index ITO. The lower index material limits the scattering angles in the GaP. (c) The GaP substrate is replaced with glass so that the ITO is the main absorber. In this case, the RMS error is 1.4%. These results demonstrate the accuracy of this method over a wide range of absorption conditions.

absorption measured for the GaP and GaP/ITO samples despite the addition of the much more absorptive ITO in the later. In this case, the ITO layer reduces the index contrast between the scattering layer and the GaP. This reduced index contrast results in only ~1/6 of the loss occurring in the scattering material. Continuing with the comparison between the GaP and GaP/ITO samples, notice the large difference in the predicted Lambertian absorption for the GaP and GaP/ITO. Lambertian scattering is defined by complete randomization in the material into which the scattering occurs; either GaP or ITO in these examples. For the GaP/ITO sample, light is scattered in a full 2π steradians in the low index ITO but this is reduced to a critical angle inside the GaP. This reduction in angle results in a much shorter average path length in the GaP and less trapped light. In contrast, for the sample with GaP alone, light is scattered in a full 2π steradians in the high index GaP resulting in a longer average path length and a greater fraction of trapped light. Finally, note the large absorption in the Glass/ITO sample compared to the GaP/ITO sample, despite a thicker ITO layer on the GaP/ITO sample. This effect is simply due to greater intrinsic absorptivity of the ITO at short wavelengths.

V. CONCLUSIONS

Here, we have demonstrated an accurate method for measuring scattering from random dielectric nanoparticles. This technique was required to evaluate the scattering into guided modes of planar structures, which would normally be inaccessible. This method was further motivated by large discrepancies between measured absorption and predictions based on typical light trapping theories for dielectric scatterers (i.e., the Lambertian and focused Lambertian models). We found that the measured scattering distribution could not be explained by the typical focused Lambertian distribution despite the fact that angle-integrated absorption data could be fit using this model. We instead proposed that the underlying cause of this distribution was the scattering from an ensemble of indices. We found that by using this model, we could accurately explain our new scattering data and precisely predict the measured absorption data.

This work has several broader implications. First, we note that this technique for the measurement of scattering distributions is not limited to dielectric scatterers. In fact, as long as near field scattering and surface modes do not play a major role, and as long as an appropriate weakly absorbing hemisphere is available for the wavelength and index range of interest, this technique can be implemented to fully characterize any scattering surface including textured surfaces or gratings by applying these structures to a suitable hemisphere. Near field scattering (including evanescent fields from surface modes) will contribute to absorption but, by definition, cannot be detected directly in the far field, and thus this scattering is outside the reach of measurements using this method. While surface modes may still refract into free-space at the edge of the hemisphere, the experiment presented here is not designed to distinguish these rays. These techniques are completely agnostic to the nature of the scattering object (size, shape, and origin) all that is required is that the hemisphere can support all the wave vectors (modes) available to the scatterer. Second, our model demonstrates the need for careful consideration of the interface between the scattering material and absorber. Even if the remainder of the scattering layer has a lower packing fraction, significant gains can be achieved by ensuring a high effective index profile near the surface.

[1]P. Campbell and M. A. Green, J. Appl. Phys. 62, 243 (1987).
[2]V. E. Ferry, J. N. Munday, and H. A. Atwater, Adv. Mater. 22, 4794 (2010).

[This article is copyrighted as indicated in the article. Reuse of AIP content is subject to the terms at: http://scitation.aip.org/termsconditions. Downloaded to] IP: 73.212.41.40 On: Sat, 16 Jan 2016 13:42:15

[3]H. Tan, L. Sivec, B. Yan, R. Santbergen, M. Zeman, and A. H. M. Smets, Appl. Phys. Lett. **102**, 153902 (2013).
[4]Z. Yu, A. Raman, and S. Fan, Opt. Express **18**, A366 (2010).
[5]M. L. Brongersma, Y. Cui, and S. Fan, Nat. Mater. **13**, 451 (2014).
[6]R. A. Pala, J. S. Q. Liu, E. S. Barnard, D. Askarov, E. C. Garnett, S. Fan, and M. L. Brongersma, Nat. Commun. **4**, 2095 (2013).
[7]R. Yan, D. Gargas, and P. Yang, Nat. Photonics **3**, 569 (2009).
[8]Y.-R. Lin, H.-P. Wang, C.-A. Lin, and J.-H. He, J. Appl. Phys. **106**, 114310 (2009).
[9]Z. Y. Wang, R. J. Zhang, S. Y. Wang, M. Lu, X. Chen, Y. X. Zheng, L. Y. Chen, Z. Ye, C. Z. Wang, and K. M. Ho, Sci. Rep. **5**, 7810 (2015).
[10]B. Wang and P. W. Leu, Nanotechnology **23**, 194003 (2012).
[11]K. X. Wang, Z. Yu, V. Liu, Y. Cui, and S. Fan, Nano Lett. **12**, 1616 (2012).
[12]E. Garnett and P. Yang, Nano Lett. **10**, 1082 (2010).
[13]A. Basch, F. Beck, T. Söderström, S. Varlamov, and K. R. Catchpole, Prog. Photovoltaics: Res. Appl. **20**, 837 (2012).
[14]Z. Ouyang, X. Zhao, S. Varlamov, Y. Tao, J. Wong, and S. Pillai, Prog. Photovoltaics: Res. Appl. **19**, 917 (2011).
[15]B. G. Lee, P. Stradins, D. L. Young, K. Alberi, T.-K. Chuang, J. G. Couillard, and H. M. Branz, Appl. Phys. Lett. **99**, 064101 (2011).
[16]B. Lipovšek, J. Krč, O. Isabella, M. Zeman, and M. Topič, J. Appl. Phys. **108**, 103115 (2010).
[17]W. E. Vargas, A. Amador, and G. A. Niklasson, Opt. Commun. **261**, 71 (2006).
[18]M. C. W. van Rossum and T. M. Nieuwenhuizen, Rev. Mod. Phys. **71**, 313 (1999).
[19]P. Nitz, J. Ferber, R. Stangl, H. Rose Wilson, and V. Wittwer, Sol. Energy Mater. Sol. Cells **54**, 297 (1998).
[20]W. E. Vargas, P. Greenwood, J. E. Otterstedt, and G. A. Niklasson, Sol. Energy **68**, 553 (2000).
[21]A. Lin, S. M. Fu, Y. K. Zhong, C. W. Tseng, P. Y. Chen, and N. P. Ju, J. Appl. Phys. **115**, 153105 (2014).
[22]J. E. Cotter, J. Appl. Phys. **84**, 618 (1998).
[23]M. A. Green, Prog. Photovoltaics: Res. Appl. **10**, 235 (2002).
[24]E. Yablonovitch, J. Opt. Soc. Am. **72**, 899 (1982).
[25]E. Yablonovitch and G. D. Cody, IEEE Trans. Electron Devices **29**, 300 (1982).
[26]C. L. Butner, J. B. Schutt, and M. C. Shai, Appl. Opt. **23**, 1139 (1984).
[27]U. Rau, U. W. Paetzold, and T. Kirchartz, Phys. Rev. B **90**, 035211 (2014).
[28]Z. Yu, N. P. Sergeant, T. Skauli, G. Zhang, H. Wang, and S. Fan, Nat. Commun. **4**, 1730 (2013).
[29]C. C. Katsidis and D. I. Siapkas, Appl. Opt. **41**, 3978 (2002).

[This article is copyrighted as indicated in the article. Reuse of AIP content is subject to the terms at: http://scitation.aip.org/termsconditions. Downloaded to] IP: 73.212.41.40 On: Sat, 16 Jan 2016 13:42:15